Borneo Journal of Pharmacy
Vol 9 Issue 1 March 2026
Pages 77 – 87

https://journal.umpr.ac.id/index.php/bjop/article/view/10948
DOI: https://doi.org/10.33084/bjop.v9i1.10948
e-ISSN: 2621-4814

Research Article

Molecular Docking and QSAR Analysis of *N*-(Ethylcarbamothioyl)benzamide Derivatives as Dual Estrogen-Alpha and Progesterone Receptors Inhibitor for Breast Cancer

Anung Kustriyani [1]

Bambang Tri Purwanto [2,3*]

Tri Widiandani [2,3]

Khoirunnisa Muslimawati [4]

[1] Doctoral Program of Pharmaceutical Sciences, Universitas Airlangga, Surabaya, East Java, Indonesia
[2] Department of Pharmaceutical Sciences, Universitas Airlangga, Surabaya, East Java, Indonesia
[3] Research Group of Drug Development, Universitas Airlangga, Surabaya, East Java, Indonesia
[4] Pharmacist Professional Education Study Program, Universitas Lambung Mangkurat, Banjarbaru, South Kalimantan, Indonesia

*email: bambang-t-p@ff.unair.ac.id; phone: +628123536513

Keywords:
Breast cancer
In silico
Molecular docking
N-(Ethylcarbamothyoil)benzamide derivatives
Quantitative structure-activity relationship

Abstract

Luminal A subtype breast cancer is the most prevalent disease suffered by women, characterized by the presence of positive hormone receptors in the form of estrogen and progesterone. Thiourea derivatives have been shown to exhibit cytotoxicity against breast cancer cells *in silico* across multiple receptor targets. The purpose of this study was to determine the binding energy and QSAR equation of *N*-(Ethylcarbamothioyl)benzamide derivatives *in silico*. Molecular docking of the compounds was performed using AutoDockTools-1.5.7 with estrogen-α (PDB ID: 3ERT) and progesterone (PDB ID: 2OVM) receptor targets. The results showed that the compound 4-(benzyloxy)-*N*-(ethylcarbamothioyl)benzamide had the smallest free energy of binding (ΔG) and K_i on estrogen-α and progesterone receptor of -7.13 kcal/mol and 5.96 µM and -8.04 kcal/mol and 1.27 µM, respectively. The best QSAR equation for estrogen-α receptor is $\Delta G = 0.465\ (LogP)^2 - 2.276\ logP + 0.311\ E_{LUMO} - 0.091\ MR + 5.075$ ($R = 0.914$, $\alpha < 0.001$, $F = 16.595$ and $SE = 0.41331$) and progesterone receptor is $\Delta G = -0.058\ (LogP)^2 - 0.033\ tPSA + 0.011\ E_{tot} - 0.08\ MR + 1.683$ ($R = 0.92$, $\alpha < 0.001$, $F = 18.028$ and $SE = 0.37388$). The QSAR equation is statistically significant if the R-squared value approaches 1, significance ($\alpha < 0.05$), $F_{count} > F_{table}$, and the smallest standard deviation (s). The predicted physicochemical properties that influence cytotoxic activity at the estrogen-α receptor are lipophilic (logP), electronic (E_{LUMO}), and steric (MR). In contrast, those at the progesterone receptor are lipophilic (tPSA), electronic (E_{tot}), and steric (MR).

Received: September 22nd, 2025
1st Revised: November 12th, 2025
Accepted: December 11th, 2025
Published: March 30th, 2026

INTRODUCTION

Breast cancer is fundamentally characterized by deregulated cellular proliferation and is clinically classified by the presence or absence of specific hormone receptor markers, including estrogen receptor (ER), progesterone receptor (PR), and human epidermal growth factor receptor 2 (HER2)[1]. The expression profiles of these biological receptors define distinct luminal breast cancer subtypes, directly influencing the subsequent selection of targeted therapeutic regimens[2]. Among these variants, the Luminal A subtype exhibits the highest clinical incidence, accounting for approximately 40% of all diagnosed cases compared to Luminal B, HER2-enriched, and triple-negative breast cancer (TNBC) cohorts[3]. Pathological features of Luminal A include an ER-positive (ER+), PR-positive (PR+), and human epidermal growth factor receptor 2-negative (HER2-) signature, alongside a Ki-67 proliferation index of less than 20%, a favorable clinical prognosis, and a distinct absence of aggressive mutational cascades, rendering it highly responsive to conventional adjuvant hormonal interventions[4].

How to cite: Kustriyani A, Purwanto BT, Widiandani T, Muslimawati K. Molecular Docking and QSAR Analysis of N-(Ethylcarbamothioyl)benzamide Derivatives as Dual Estrogen-Alpha and Progesterone Receptors Inhibitor for Breast Cancer. Borneo J Pharm. 2026;9(1):77-87. doi:10.33084/bjop.v9i1.10948

Globally, cancer incidence metrics expand each year substantially; data from the International Agency for Research on Cancer (IARC) estimated the 2022 global burden at 20 million new cases with 9.7 million associated fatalities, with projections indicating a 77% surge to 35 million new annual cases by the year 2050. Within this epidemiological landscape, breast cancer stands as the leading malignant diagnosis among women worldwide, representing 2.3 million new cases (11.6%) and resulting in 670,000 deaths (6.9%) annually[5]. Intracellularly, ER and PR receptors are constitutively expressed in 15% to 30% of normal mammary luminal epithelial cells[6]. The primary ER isoforms driving breast cancer pathophysiology are ERα and ERβ, with the ERα isoform actively expressed in up to 70% of all breast malignancies, whereas ERβ expression regularly decreases as clinical severity advances, underscoring its role as a ligand-activated tumor suppressor. Furthermore, functional PR is expressed in more than 60% of ER+ breast tumors[7].

The standard endocrine management of Luminal A subtype breast cancer heavily utilizes hormonal therapeutic modulators such as tamoxifen. Mechanistically, tamoxifen acts as a competitive antagonist of endogenous estrogens by binding to ERα, thereby suppressing downstream cancer cell proliferation and simultaneously downregulating estradiol-induced PR expression[8]. Prior computational investigations have demonstrated that tamoxifen binds to both ERα and PR, with distinct binding affinities during *in silico* molecular docking simulations[9]. Complementary research workflows have also targeted various secondary metabolites capable of binding and inhibiting these two core receptors *in silico*, positioning them as viable candidates for chemoprevention strategies[10].

Concurrently, thiourea derivatives have emerged as key pharmacophores with robust cytotoxic activity against breast cancer cell lines in both *in silico* and *in vitro* assays[11]. Automated *in silico* screenings of these derivatives have identified multiple target boundaries, including HER2, EGFR, and SIRT-1 complexes[12,13]. The underlying anticancer profile of the thiourea framework is driven by its essential core pharmacophores, specifically the sulfur (S) and nitrogen (NH) atoms, alongside the structural optimization of functional substituents arranged at the 1 and 3 positions of the thiourea scaffold[14]. Empirical evaluations have shown that thiourea derivatives functionalized with chlorine (Cl) and fluorine (F) atoms bound to peripheral aromatic rings exhibit enhanced *in vitro* cytotoxicity[15,16]. Incorporating a halogen atom, such as Cl, into the aromatic architecture acts as an inductive electron-withdrawing group, enhancing molecular lipophilicity and directly increasing cytotoxic efficacy in MTT cell viability assays[17]. Similarly, the integration of benzoyl and methyl structural groups onto the thiourea backbone increases overall anticancer activity compared to basic hydroxyurea models that lack a benzoyl ring system, while the addition of a nitro group (–NO_2) acts as a powerful structural electron-withdrawing moiety[18].

The specific compound *N*-(Ethylcarbamothioyl)benzamide and its structural derivatives possess a common layout, with a core S and NH atom, integrated aromatic rings, and accessible substituent sites for Cl, –CH_3, –NO_2, and F groups on the phenyl ring system. Based on these topological attributes, it is possible to map and predict the potential anticancer efficacy of *N*-(Ethylcarbamothioyl)benzamide derivatives using *in silico* modeling methods. Consequently, this study uses molecular docking simulations to evaluate a series of *N*-(Ethylcarbamothioyl)benzamide derivatives for their capacity to inhibit ERα (PDB ID: 3ERT) and PR (PDB ID: 2OVM) using AutoDock software to calculate their comparative free binding energies (ΔG). The selection of these specific PDB crystallographic coordinates was based on the structural alignment of their respective native co-crystallized ligand, 4-hydroxytamoxifen (4OHT). Preliminary control simulations established that the baseline ΔG metrics for the native 4OHT compound against ERα and PR are -11.35 kcal/mol and -9.80 kcal/mol, respectively.

MATERIALS AND METHODS

Materials

The computational materials used in this study comprised the two- and three-dimensional molecular structures, along with the canonical SMILES codes for 4OHT, *N*-(Ethylcarbamothioyl)benzamide, and its structural derivatives. The crystallographic coordinates for the target macromolecules, specifically ERα and PR, were retrieved from the RCSB Protein Data Bank using the PDB identifiers 3ERT and 2OVM, respectively. Molecular modeling, structure drawing, and geometric optimizations were performed using ChemBioDraw Ultra 2D and 3D version 20.0. *In silico* physicochemical descriptors, including partition coefficients (LogP) and molecular weights, were computed using the pkCSM online platform, while structural line notations were processed via the CACTUS online SMILES generator. Graphical visualizations of ligand-

receptor interactions and amino acid residue mapping were conducted using Discovery Studio 2021. Molecular docking simulations were performed using AutoDockTools 1.5.7 on a Windows 10 system with an Intel Core i5 processor and 256 GB of memory, while downstream quantitative structure-activity relationship (QSAR) modeling and statistical regression were performed using IBM SPSS version 27.0[19-21].

Methods

Macromolecular target selection and receptor preparation

The target receptor structures for 3ERT and 2OVM were prepared by removing all co-crystallized water molecules and non-essential heteroatoms from the protein matrix. Polar hydrogen atoms were added to the target structures, missing atoms were repaired, and Gasteiger-type electrical balances were assigned by computing Kollman charges before exporting the final macromolecular structures in PDB format. The selection of these specific PDB crystallographic coordinates was based on the structural alignment of their respective native co-crystallized ligand (4OHT)[21].

Ligand sketching, structural optimization, and geometric minimization

Candidate ligand structures were sketched in 2D using ChemBioDraw Ultra version 20.0, structurally refined using the built-in "Clean Up Structure" algorithm, and subsequently transferred into the ChemBioDraw Ultra 3D module. Energy minimization was performed using the MMFF94 force field to obtain the lowest possible conformer energy. The optimized ligand geometries were saved in SMILES (.smi), SYBYL (.mol2), and SDFile (*.sdf) formats, and the final docking inputs were converted to the standard PDBQT format, with configuration methods documented in the DPF and GPF file formats[21].

Re-docking protocol and spatial method validation

Prior to screening the novel derivatives, the docking protocol was validated via a cross-validation re-docking procedure to ensure accuracy. The method was considered valid if the Root Mean Square Deviation (RMSD) between the computed pose and the co-crystallized pose of the native ligand was less than 2 Å. The native control ligands used for validation were 4OHT for 3ERT and 4-[(11β,17β)-17-methoxy-17-(methoxymethyl)-3-oxoestra-4,9-dien-11-yl]benzaldehyde oxime for 2OVM[22].

Production molecular docking and active site grid parametrization

Production docking runs between the targets and the prepared MOL2 files of 4OHT, *N*-(Ethylcarbamothioyl)benzamide, and its derivatives were performed using AutoDockTools-1.5.7. The simulations used a defined grid box of 40 x 40 x 40 $Å^3$, with a spatial resolution of 0.375 Å, centered at x = 30.282, y = -1.913, and z = 24.206 to encapsulate the active binding pocket, with the ligand positioned at the center. The primary binding outputs were recorded as ΔG (kcal/mol) and inhibition constants (K_i), while the specific participating pocket amino acid residues were evaluated using Discovery Studio Visualizer[22].

Quantitative structure-activity relationship descriptor modeling

Linear and non-linear regression equations for the QSAR modeling of *N*-(Ethylcarbamothioyl)benzamide derivatives against both target receptors were developed using IBM SPSS. The independent variables comprised lipophilic descriptors (LogP and tPSA), electronic properties (total energy, E_{tot}, and lowest unoccupied molecular orbital energy, E_{LUMO}), and steric parameters (molecular weight, MW, and molecular refractivity, MR), which were evaluated to identify their relationship with the calculated docking affinity (ΔG). The required descriptor metrics were compiled from the pkCSM online platform (LogP and MR), ChemBioDraw Ultra 2D (tPSA and MR), and ChemBioDraw Ultra 3D (E_{tot} and E_{LUMO})[23].

Data analysis

The quantitative data generated from the docking simulations and descriptor calculations were organized into structured tabular matrices. The resulting QSAR regression equations were evaluated against standard statistical thresholds to assess model validity. The QSAR equations met the required criteria if the correlation coefficient (r) approached 1.0, the significance value (sig.) satisfied $\alpha < 0.05$, the calculated F-statistic was greater than the critical F-value, and the standard deviation (s) was the lowest possible[19,23].

RESULTS AND DISCUSSION

The *in silico* investigation began with the generation of the initial 2D geometries of the core compounds. **Figure 1** illustrates the optimized topologies of 4OHT, the parent *N*-(Ethylcarbamothioyl)benzamide scaffold, and its representative halogenated derivative, 3,4-dichloro-*N*-(ethylcarbamothioyl)benzamide. Following structure generation, systematic molecular docking simulations of the *N*-(Ethylcarbamothioyl)benzamide derivatives were performed using AutoDockTools-1.5.7. The resulting structural poses were analyzed using four primary criteria: RMSD values, ΔG, K_i, and spatial amino acid residue interactions. The comprehensive docking metrics for the native control and the seventeen newly designed derivatives (NE1–NE17) against both hormone receptors are compiled in **Table I**.

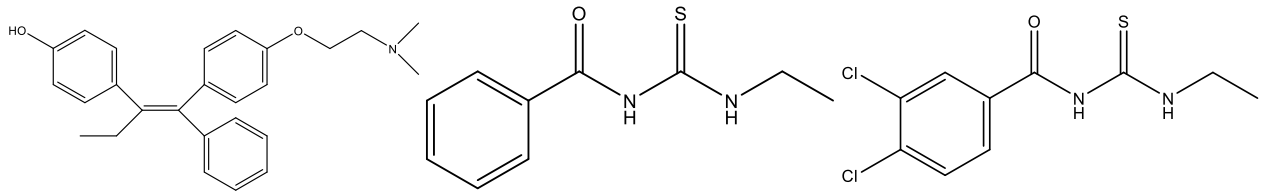

a **b** **c**

Figure 1. 2D structure of the compound: (**a**) 4OHT, (**b**) *N*-(Ethylcarbamothioyl)benzamide, (**c**) 3,4-dichloro-*N*-(ethylcarbamothioyl)benzamide.

Table I. ΔG and K_i values of 4OHT and *N*-(Ethylcarbamothioyl)benzamide derivatives.

Code	Substituents	Chemical Compound	ERα (3ERT)			PR (2OVM)		
			RMSD (Å)	ΔG (kcal/mol)	Ki (μM)	RMSD (Å)	ΔG (kcal/mol)	Ki (μM)
4OHT	-OH	4-hydroxytamoxifen	1.117	-11.35	4.77×10^{-3}	1.062	-9.80	65.06×10^{-3}
NE	-	*N*-(Ethylcarbamothioyl)benzamide	1.125	-4.36	636.29	1.046	-5.15	168.29
NE1	3,4-Cl_2	3,4-dichloro-*N*-(ethylcarbamothioyl)benzamide	1.149	-4.82	295.36	1.067	-6.33	22.98
NE2	3,4-$(CF_3)_2$	*N*-(ethylcarbamothioyl)-3,4-bis(trifluoromethyl)benzamide	1.062	-4.77	318.88	1.051	-5.93	45.35
NE3	2,4-Cl_2	2,4-dichloro-*N*-(ethylcarbamothioyl)benzamide	1.259	-4.61	417.25	1.069	-6.25	26.35
NE4	4-$C(CH_3)_3$	4-(tert-butyl)-*N*-(ethylcarbamothioyl)benzamide	1.153	-5.79	57.05	1.030	-6.96	7.90
NE5	3,4-$(CH_3)_2$	*N*-(ethylcarbamothioyl)-3,4-dimethylbenzamide	1.040	-4.94	241.14	1.073	-6.01	39.26
NE6	4-$OCH(CH_3)_2$	*N*-(ethylcarbamothioyl)-4-isopropoxybenzamide	0.970	-5.80	55.85	1.033	-6.54	16.20
NE7	4-OCH_2Ph	4-(benzyloxy)-*N*-(ethylcarbamothioyl)benzamide	1.072	-7.13	5.96	1.063	-8.04	1.27
NE8	4-OPh	*N*-(ethylcarbamothioyl)-4-phenoxybenzamide	1.158	-6.60	13.09	1.062	-7.23	5.01
NE9	3,5-Cl_2	3,5-dichloro-*N*-(ethylcarbamothioyl)benzamide	1.090	-4.94	237.79	1.066	-5.67	70.15
NE10	3,5-$(CF_3)_2$	*N*-(ethylcarbamothioyl)-3,5-bis(trifluoromethyl)benzamide	1.301	-4.93	243.19	1.052	-5.43	105.05
NE11	3-NO_2	*N*-(ethylcarbamothioyl)-3-nitrobenzamide	1.114	-4.66	383.72	1.081	-7.02	7.14
NE12	4-F	*N*-(ethylcarbamothioyl)-4-fluorobenzamide	1.055	-4.34	655.78	0.977	-5.13	172.88
NE13	3-$N(CH_3)_2$	3-(dimethylamino)-*N*-(ethylcarbamothioyl)benzamide	1.137	-5.04	202.92	0.968	-5.77	58.50
NE14	2-Cl	2-chloro-*N*-(ethylcarbamothioyl)benzamide	1.251	-4.19	846.10	1.057	-5.21	152.83
NE15	2-CH_3	*N*-(ethylcarbamothioyl)-2-methylbenzamide	1.096	-4.01	1160.00	1.070	-5.13	173.02
NE16	2-OCH_3	*N*-(ethylcarbamothioyl)-2-methoxybenzamide	1.064	-3.90	1390.00	0.982	-5.41	109.12
NE17	4-$N(CH_3)_2$	4-(dimethylamino)-*N*-(ethylcarbamothioyl)benzamide	1.084	-3.89	1400.00	1.075	-5.63	75.24

Prior to conducting production docking runs, the co-crystallized native ligand was validated to confirm grid precision. The cross-validation protocol yielded RMSD values ranging from 0.970 to 1.301 Å for ERα and from 0.968 to 1.081 Å for PR. Because all computed RMSD entries fell safely below the standard 2.0 Å threshold, the docking grid configuration

demonstrated sufficient accuracy. RMSD limits are widely used to assess how closely a predicted *in silico* model aligns with empirical crystallographic structures, with values below 2.0 Å indicating reliable structural reproducibility[24].

The synthesized *N*-(Ethylcarbamothioyl)benzamide derivatives exhibited calculated ΔG spanning from -4.34 to -7.13 kcal/mol against ERα, and -5.13 to -8.04 kcal/mol against PR. The derivative 4-(benzyloxy)-*N*-(ethylcarbamothioyl)benzamide (NE7) demonstrated the highest binding affinity across both macro-receptors, recording lowest energy scores of -7.13 kcal/mol and -8.04 kcal/mol, respectively. Thermodynamic binding energy describes the net potential driving force required for an exogenous ligand to stabilize within a targeted receptor cleft; highly negative ΔG values indicate enhanced stability and stronger intermolecular affinity. In structure-based drug design, these energy values provide predictive metrics to map ligand affinities, identify promising hit candidates, and optimize lead structures by estimating how well a molecule fits the active site topology[25].

Correspondingly, the computed K_i for the derivative library ranged from 5.96 to 1400 µM for ERα, and 1.27 to 173.02 µM for PR. Consistent with the energy metrics, compound NE7 achieved the lowest K_i values at 5.96 µM (ERα) and 1.27 µM (PR). The inhibition constant is a critical kinetic descriptor that reflects the concentration of an antagonist required to reduce enzyme or receptor activation by half; lower K_i values indicate that lower drug concentrations are needed to achieve receptor saturation[26]. Molecules with high thermodynamic affinities naturally demonstrate lower K_i thresholds. This relationship is governed by the equation $K_i = \exp(\Delta G/RT)$, where R is the universal gas constant, and T is the absolute temperature. Consequently, an increasingly negative ΔG directly scales the exponential K_i index down, confirming a tighter ligand-target complex[27].

The spatial orientations and atomic contacts linking these ligands to the active sites of ERα (3ERT) and PR (2OVM) are mapped in **Figure 2**. The interaction profile for the high-affinity compound 4-(benzyloxy)-*N*-(ethylcarbamothioyl)benzamide (NE7) within the ERα active site includes a distinct hydrogen bond at AspA:351, supported by non-bonded steric contacts across ThrA:347, AspA:351, MetA:343, LeuA:346, TrpA:383, LeuA:387, LeuA:354, AlaA:350, LeuA:525, and MetA:421. Within the PR cleft, NE7 anchors via multiple hydrogen bonds at TyrA:890, CysA:891, and GlnA:725, balanced by steric stabilization at MetA:756, PheA:778, LeuA:763, LeuA:887, MetA:801, and MetA:759. The hydrogen-bonding network of NE7 is notably more extensive in the PR target than in ERα. This structural difference aligns with the computed ΔG values, which favor PR target (-8.04 kcal/mol) over ER complex (-7.13 kcal/mol), as localized hydrogen bonds stabilize the bound-state conformation[28]. When contrasted with the high-affinity profile of NE7, the low-affinity derivative 4-(dimethylamino)-*N*-(ethylcarbamothioyl)benzamide (NE17) forms fewer directional contacts with surrounding amino acids. Structurally, ΔG is derived from a balance of internal ligand-protein energies and conformational entropy losses upon binding[29]. The superior performance of NE7 is largely driven by its dual benzene rings, which enhance hydrophobic interactions and boost overall cytotoxic potential[30].

To build a descriptive QSAR framework, the lipophilic, electronic, and steric properties of the derivatives were evaluated. The structural parameters gathered in **Table II** serve as independent molecular descriptors for the mathematical QSAR modeling. These lipophilic, electronic, and steric indices are essential for predicting drug-likeness profiles alongside ADMET pharmacokinetic parameters. Lipophilicity scales describe a molecule's capacity to traverse lipid bilayers, which is frequently quantified by LogP and tPSA values[31]. Electronic variables reflect molecular charge distribution and target-binding tendencies, captured here by E_{tot} and E_{LUMO}. Steric properties, including molecular volume and spatial boundaries that dictate contact with the active site pocket, are represented by MW and MR[32]. According to the standard rule-of-five criteria, a candidate molecule is considered drug-like when its LogP is less than or equal to 5, its MW is less than or equal to 500 g/mol, and its tPSA is less than or equal to 140 Å for effective passive membrane absorption[33]. The evaluated *N*-(Ethylcarbamothioyl)benzamide derivatives systematically met these drug-likeness thresholds.

Linear and non-linear polynomial regression models were constructed by correlating computed docking affinities against the lipophilic, electronic, and steric descriptors of the series. The generated QSAR models identify key physicochemical parameters that influence the predicted cytotoxic profiles. The resulting equations are detailed in **Table III**. The mathematical QSAR outputs isolate specific lipophilic, electronic, and steric configurations that directly govern interactions within the target binding pocket. For the ERα dataset, the top-performing QSAR model is represented by Equation 19: $\Delta G = 0.465\ (\text{LogP})^2 - 2.276\ \text{logP} + 0.311\ E_{LUMO} - 0.091\ \text{MR} + 5.075$, which achieved an r value of 0.914, significance under 0.001, a calculated F-statistic of 16.595 (exceeding the critical table value of 3.18), and a standard error of 0.41331. For the progesterone dataset, the optimal mathematical fit is also captured by Equation 19: $\Delta G = -0.058\ (\text{LogP})^2 - 0.033\ \text{tPSA} + 0.011\ E_{tot} - 0.080\ \text{MR}$

+ 1.683, yielding an r value of 0.920, significance under 0.001, an F-statistic of 18.028 (critical table value of 3.18), and a minimized standard error of 0.37388. Within these mathematical frameworks, positive descriptor coefficients indicate a direct relationship with the dependent variable, whereas negative values indicate an inverse relationship.

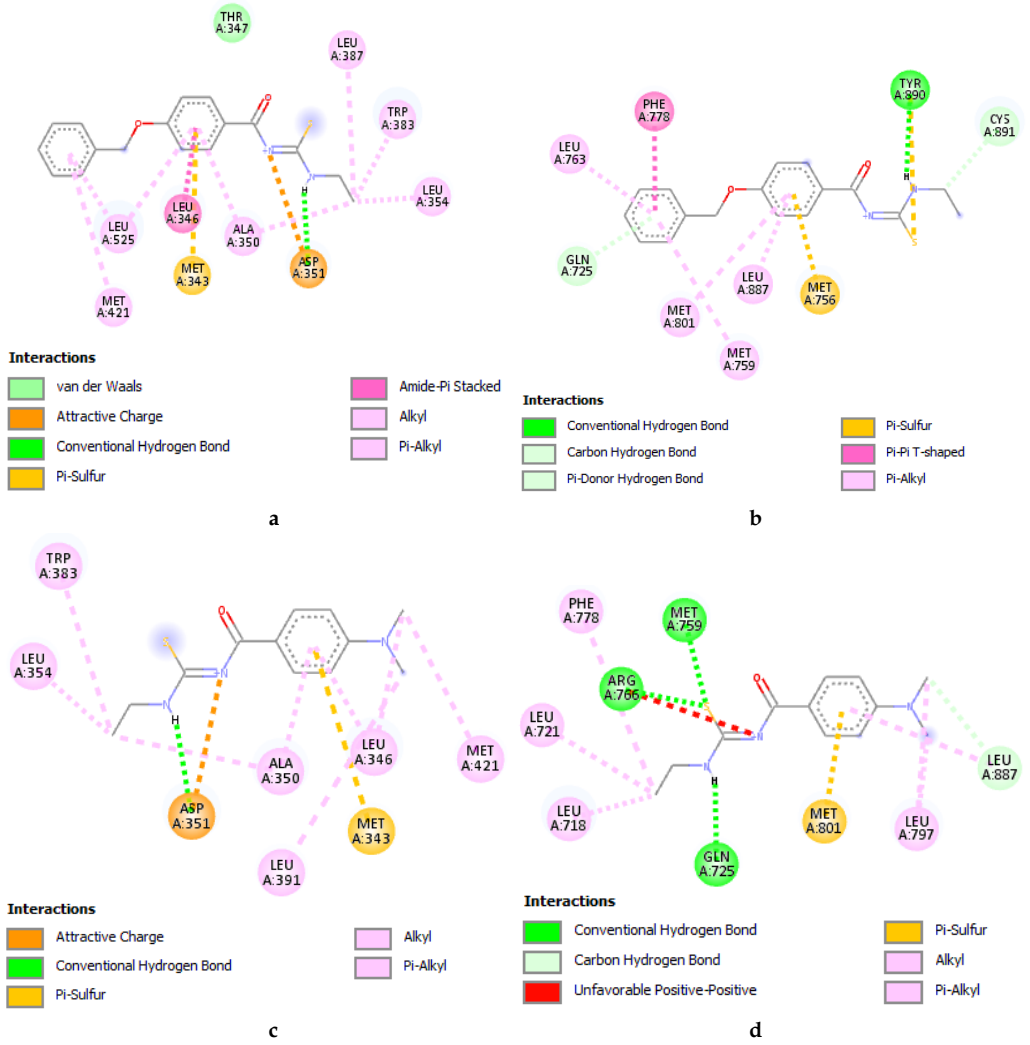

Figure 2. 2D Interactions receptor and ligand 4-(benzyloxy)-*N*-(ethylcarbamothioyl)benzamide and 4-(dimethylamino)-*N*-(ethylcarbamothioyl)benzamide, respectively: (**a** and **c**) on ERα (3ERT); (**b** and **d**) and on the progesterone (2OVM) receptor *in silico*.

Table II. Lipophilic, electronic, and steric properties of *N*-(Ethylcarbamothioyl)benzamide derivatives.

Code	LogP	tPSA (Å)	E_{tot} (kcal/mol)	E_{LUMO}	MW (g/mol)	MR (cm³/mol)
NE	1.3108	41.13	-27.2652	-3.755	208.286	59.30
NE1	2.6176	41.13	-27.0603	-2.868	277.176	68.51
NE2	3.3484	41.13	3.97915	-3.582	344.280	72.31
NE3	2.6176	41.13	-39.4137	-2.472	277.176	68.51
NE4	2.6083	41.13	-9.27326	-3.337	264.394	78.97
NE5	1.9276	41.13	-21.2280	-3.428	236.340	71.09
NE6	2.0980	50.36	-14.8710	-2.913	266.366	76.03
NE7	2.8898	50.36	1.77989	-2.917	314.410	91.04
NE8	3.1031	50.36	-2.93193	-2.904	300.383	85.63
NE9	2.6176	41.13	-53.0551	-3.542	277.176	68.51
NE10	3.3484	41.13	20.1118	-3.703	344.280	72.31
NE11	1.2190	92.94	-4.7893	-5.013	253.283	68.47
NE12	1.4499	41.13	-29.5256	-2.811	226.276	59.70
NE13	1.3768	44.37	-28.2963	-3.587	251.355	74.48
NE14	1.9642	41.14	-31.5068	-3.284	242.731	63.90
NE15	1.61922	41.13	-24.1695	-3.541	222.313	65.19
NE16	1.3194	50.36	-21.9838	-3.401	238.312	66.54
NE17	1.3768	44.37	-25.6970	-1.424	251.355	74.48

Table III. QSAR equation of *N*-(Ethylcarbamothioyl)benzamide derivatives on ERα and PR.

No.	Target and QSAR Model	R	Sig	F-statistic	SE
	ERα				
1	$\Delta G = -0.012\ MW - 1.777$	0.516	0.029	5.793	0.78881
2	$\Delta G = -0.095\ MR + 1.845$	0.864	<0.001	46.937	0.46417
3	$\Delta G = 0.561\ logP - 0.012\ E_{tot} - 3.939$	0.610	0.031	4.436	0.75368
4	$\Delta G = -0.196\ logP - 0.085\ MR + 1.588$	0.875	<0.001	24.443	0.46071
5	$\Delta G = -0.000\ tPSA - 0.095\ MR + 1.849$	0.864	<0.001	22.002	0.47939
6	$\Delta G = -0.209\ logP + 0.002\ E_{tot} - 0.087\ MR + 1.782$	0.875	<0.001	15.314	0.47562
7	$\Delta G = -0.190\ logP + 0.222\ E_{LUMO} - 0.090\ MR + 2.638$	0.892	<0.001	18.088	0.44569
8	$\Delta G = (-9.019 \times 10^{-5})\ tPSA - (6.480 \times 10^{-5})\ E_{tot} - 0.095\ MR + 1.842$	0.864	<0.001	13.690	0.49622
9	$\Delta G = 0.011\ tPSA + 0.335\ E_{LUMO} - 0.0103\ MR + 3.039$	0.890	<0.001	17.703	0.44952
10	$\Delta G = 0.0351\ (LogP)^2 - 2.257\ LogP - 1.881$	0.597	0.037	4.148	0.76296
11	$\Delta G = -0.163\ (LogP)^2 - 0.018\ tPSA - 3.229$	0.602	0.034	4.258	0.75938
12	$\Delta G = -0.116\ (LogP)^2 - 0.011\ E_{tot} - 4.533$	0.580	0.046	3.802	0.77455
13	$\Delta G = -0.037\ (LogP)^2 - 0.087\ MR + 1.470$	0.872	<0.001	23.722	0.46600
14	$\Delta G = 1.080\ (LogP)^2 - 5.197\ logP - 0.030\ E_{tot} + 0.124$	0.720	0.014	5.013	0.68334
15	$\Delta G = 0.297\ (LogP)^2 - 1.529\ logP - 0.085\ MR + 2.876$	0.885	<0.001	16.937	0.45741
16	$\Delta G = -0.043\ (LogP)^2 - 0.004\ tPSA - 0.085\ MR + 1.543$	0.873	<0.001	14.954	0.47998
17	$\Delta G = 1.246\ (LogP)^2 - 5.645\ logP - 0.029\ E_{tot} - 0.007\ MW + 2.034$	0.726	0.034	3.620	0.70246
18	$\Delta G = 0.481\ (LogP)^2 - 2.310\ logP - 0.007\ E_{tot} - 0.078\ MR + 3.009$	0.890	<0.001	12.328	0.46650
19	$\Delta G = 0.465\ (LogP)^2 - 2.276\ logP + 0.311\ E_{LUMO} - 0.091\ MR + 5.075$	0.914	<0.001	16.595	0.41331
20	$\Delta G = -0.056\ (LogP)^2 - 0.007\ tPSA + 0.005\ E_{tot} - 0.087\ MR + 1.997$	0.876	<0.001	10.716	0.49269
21	$\Delta G = -0.019\ (LogP)^2 + 0.008\ tPSA + 0.303\ E_{LUMO} - 0.098\ MR + 2.788$	0.891	<0.001	12.537	0.46340
	Progesterone				
1	$\Delta G = -0.085\ MR + 0.047$	0.829	<0.001	35.241	0.48186
2	$\Delta G = 0.042\ logP - 0.087\ MR + 0.101$	0.830	<0.001	16.596	0.49686
3	$\Delta G = -0.031\ tPSA - 0.010\ MW - 1.990$	0.632	0.022	5.000	0.68985
4	$\Delta G = -0.024\ tPSA - 0.081\ MR + 0.893$	0.901	<0.001	32.280	0.38670
5	$\Delta G = 0.042\ logP - (6.926 \times 10^{-5})\ E_{tot} - 0.087\ MR$	0.830	<0.001	10.327	0.51430
6	$\Delta G = 0.048\ logP + 0.248\ E_{LUMO} - 0.093\ MR + 1.273$	0.855	<0.001	12.681	0.47813
7	$\Delta G = -0.031\ tPSA - 0.001\ E_{tot} - 0.010\ MW - 2.058$	0.633	0.060	3.112	0.71402
8	$\Delta G = -0.026\ tPSA + 0.006\ E_{tot} - 0.088\ MR + 1.525$	0.906	<0.001	21.499	0.38931
9	$\Delta G = -0.042\ tPSA - 0.361\ E_{LUMO} - 0.010\ MW - 2.657$	0.684	0.028	4.108	0.67228
10	$\Delta G = -0.024\ tPSA + 0.005\ E_{LUMO} - 0.082\ MR + 0.912$	0.901	<0.001	20.087	0.40026
11	$\Delta G = 0.014\ (LogP)^2 - 0.088\ MR + 0.187$	0.831	<0.001	16.691	0.49589
12	$\Delta G = 0.225\ (LogP)^2 - 0.966\ logP - 0.087\ MR + 1.075$	0.835	<0.001	10.939	0.49120
13	$\Delta G = -0.140\ (LogP)^2 - 0.041\ tPSA + 0.002\ E_{tot} - 3.396$	0.665	0.029	4.057	0.65420
14	$\Delta G = -0.142\ (LogP)^2 - 0.054\ tPSA - 0.437\ E_{LUMO} - 4.247$	0.763	0.008	6.011	0.58210
15	$\Delta G = -0.212\ (LogP)^2 - 0.044\ tPSA + 0.007\ MW - 4.738$	0.676	0.025	4.234	0.64830
16	$\Delta G = -0.028\ (LogP)^2 - 0.027\ tPSA - 0.075\ MR + 0.694$	0.902	<0.001	21.174	0.39540
17	$\Delta G = 0.447\ (LogP)^2 - 1.911\ logP - 0.009\ E_{tot} - 0.079\ MR + 1.235$	0.865	0.002	8.085	0.45120
18	$\Delta G = 0.400\ (LogP)^2 - 1.745\ logP + 0.324\ E_{LUMO} - 0.093\ MR + 3.368$	0.875	<0.001	10.626	0.46298
19	$\Delta G = -0.058\ (LogP)^2 - 0.033\ tPSA + 0.011\ E_{tot} - 0.080\ MR + 1.683$	0.920	<0.001	18.028	0.37388
20	$\Delta G = -0.299\ (LogP)^2 - 0.066\ tPSA - 0.522\ E_{LUMO} + 0.014\ MW - 6.830$	0.778	0.012	4.985	0.60098
21	$\Delta G = -0.032\ (LogP)^2 - 0.029\ tPSA - 0.050\ E_{LUMO} - 0.073\ MR + 0.487$	0.906	<0.001	14.847	0.40541

The selection of these mathematical models was guided by standard statistical success parameters: maximizing r values toward 1.0, maintaining significance values under 0.05, confirming that computed F-values exceed critical thresholds, and minimizing standard errors[34]. Notably, the physicochemical attributes driving affinity against ERα differ from those governing the progesterone interface, particularly within the lipophilic and electronic descriptor parameters. The E_{tot}, computed geometrically in ChemBioDraw 3D, represents the internal potential energy due to bond stretching, angle bending, electrostatic interactions, and Van der Waals forces. Minimized total energy values indicate more stable conformations[35]. The E_{LUMO} is the lowest-energy level of an electron-deficient molecule; lower E_{LUMO} values indicate a greater capacity to accept electrons from adjacent donors. Together, these lipophilic and electronic descriptors serve as essential predictors of how efficiently a small molecule navigates lipid membranes, distributes within vascular compartments, and fits into target receptor binding pockets[36].

CONCLUSION

The *in silico* evaluation demonstrates that 4-(benzyloxy)-*N*-(ethylcarbamothioyl)benzamide exhibits greater thermodynamic affinity and a more negative free energy of binding when interacting with the progesterone receptor. This

reduced energy value confirms the formation of a highly stable, structurally favorable ligand-receptor complex. The QSAR models reveal that the lipophilic parameter LogP, the electronic parameter E_{LUMO}, and the steric parameter MR serve as the primary structural descriptors driving the calculated *in silico* cytotoxic activity against ERα. Conversely, tPSA, E_{tot}, and MR are key predictive variables that influence cytotoxicity at the PR interface. Future development of these derivatives requires thorough *in silico* evaluation of their toxicity and of their ADME profiles, alongside an assessment of the availability of commercial precursors, before initiating chemical synthesis. By balancing these molecular docking benchmarks, calculated cytotoxicities, predicted ADMET properties, and synthetic feasibility, the selected candidate compounds can be advanced to empirical *in vitro* evaluations using breast cancer cell-line cultures to validate their therapeutic potential.

ACKNOWLEDGMENT

The authors express their sincere gratitude to the advisor and co-advisors from the Faculty of Pharmacy at Universitas Airlangga for providing invaluable academic critique, constructive suggestions, and strategic insights throughout the development of this study.

AUTHORS' CONTRIBUTION

Conceptualization: Anung Kustriyani, Bambang Tri Purwanto, Tri Widiandani
Data curation: Anung Kustriyani
Formal analysis: Anung Kustriyani
Funding acquisition: -
Investigation: Anung Kustriyani
Methodology: Bambang Tri Purwanto, Tri Widiandani
Project administration: -
Resources: -
Software: Bambang Tri Purwanto, Tri Widiandani
Supervision: Bambang Tri Purwanto, Tri Widiandani
Validation: Bambang Tri Purwanto, Tri Widiandani, Khoirunnisa Muslimawati
Visualization: -
Writing - original draft: Anung Kustriyani
Writing - review & editing: Anung Kustriyani, Bambang Tri Purwanto, Tri Widiandani, Khoirunnisa Muslimawati

DATA AVAILABILITY

None.

CONFLICT OF INTEREST

The authors declared no conflict of interest related to this research.

REFERENCES

1. Zannetti A. Breast Cancer: From Pathophysiology to Novel Therapeutic Approaches 2.0. Int J Mol Sci. 2023;24(3):2542. DOI: 10.3390/ijms24032542; PMID: 36768866; PMCID: PMC9916418.

2. Samad MA, Ahmad I, Khan MR, Suhail M, Zughaibi TA, Al-Abbasi FA, et al. Breast Cancer: Molecular Pathogenesis and Targeted Therapy. MedComm. 2025;6(10):e70404. DOI: 10.1002/mco2.70404; PMID: 41049266; PMCID: PMC12495454.

3. Nolan E, Lindeman GJ, Visvader JE. Deciphering breast cancer: from biology to the clinic. Cell. 2023;186(8):1708-28. DOI: 10.1016/j.cell.2023.01.040; PMID: 36931265.

4. Gao JJ, Swain SM. Luminal A Breast Cancer and Molecular Assays: A Review. Oncologist. 2018;23(5):556-65. DOI: 10.1634/theoncologist.2017-0535; PMID: 29472313; PMCID: PMC5947456.

5. Bray F, Laversanne M, Sung H, Ferlay J, Siegel RL, Soerjomataram I, et al. Global cancer statistics 2022: GLOBOCAN estimates of incidence and mortality worldwide for 36 cancers in 185 countries. CA Cancer J Clin. 2024;74(3):229-63. DOI: 10.3322/caac.21834; PMID: 38572751.

6. Li Z, Wei H, Li S, Wu P, Mao X. The Role of Progesterone Receptors in Breast Cancer. Drug Des Devel Ther. 2022;16:305-14. DOI: 10.2147/DDDT.S336643; PMID: 35115765; PMCID: PMC8801368.

7. Choi Y. Estrogen Receptor β Expression and Its Clinical Implication in Breast Cancers: Favorable or Unfavorable? J Breast Cancer. 2022;25(2):75-93. DOI: 10.4048/jbc.2022.25.e9; PMID: 35380018; PMCID: PMC9065353.

8. Munzone E, Colleoni M. Optimal management of luminal breast cancer: how much endocrine therapy is long enough? Ther Adv Med Oncol. 2018;10:1758835918777437. DOI: 10.1177/1758835918777437; PMID: 29977350; PMCID: PMC6024281.

9. Chakraborty S, Biswas PK. Structural insights into selective agonist actions of tamoxifen on human estrogen receptor alpha. J Mol Model. 2014;20(8):2338. DOI: 10.1007/s00894-014-2338-x; PMID: 25060147; PMCID: PMC4379705.

10. Agamah FE, Mazandu GK, Hassan R, Bope CD, Thomford NE, Ghansah A, et al. Computational/in silico methods in drug target and lead prediction. Brief Bioinform. 2020;21(5):1663-75. DOI: 10.1093/bib/bbz103; PMID: 31711157; PMCID: PMC7673338.

11. Kesuma D, Siswandono, Kirtishanti A. Molecular docking and biological activity N-(4-Methoxy)-benzoyl-N′-phenylthiourea and N-(4-Trifluoro)-benzoyl-N′-phenylthiourea as anti-breast cancer candidates. Rasayan J Chem. 2022;15(2):1503-8. DOI: 10.31788/RJC.2022.1526836.

12. Kesuma D, Kristishanti A, Makayasa CHA, Sumartha IGA. Anticancer activity of N-(4-t-butylbenzoyl)-N′-phenylthiourea: molecular docking, synthesis, and cytotoxic activity in breast and cervical cancer cells. J Pharm Pharmacogn Res. 2023;11(2):208-15. DOI: 10.56499/jppres22.1508_11.2.208.

13. Widiandani T, Siswandono, Meiyanto E. Anticancer evaluation of N-benzoyl-3-allylthiourea as potential antibreast cancer agent through enhances HER-2 expression. J Adv Pharm Technol Res. 2020;11(4):163-8. DOI: 10.4103/japtr.JAPTR_77_20; PMID: 33425698; PMCID: PMC7784947.

14. Fayyaz A, Ejaz SA, Ahmed A, Channar PA, Afzal S, Ujan R, et al. Design, synthesis, and anticancer activity of novel isocryptolepine 'aza' type acyl thiourea derivatives via combined experimental and computational approach. Biosci Rep. 2026;46(1):BSR20253519. DOI: 10.1042/BSR20253519; PMID: 41428767; PMCID: PMC12863032.

15. Siswandono, Widiandani T, Hardjono S. Docking and cytotoxicity test on human breast cancer cell line (T47D) of N-(Allylcarbamothioyl)-3-chlorobenzamide dan N-(Allylcarbamothioyl)-3,4-dichlorobenzamide. Res J Pharm Biol Chem Sci. 2018;8(2): 1909-14.

16. Widiandani T, Siswandono S, Meiyanto E, Sulistyowaty MI, Purwanto BT, Hardjono S. New N-allylthiourea derivatives: Synthesis, molecular docking and in vitro cytotoxicity studies. Trop J Pharm Res. 2018;17(8):1607-13. DOI: 10.4314/tjpr.v17i8.20.

17. Ruswanto, Miftah AM, Tjahjono DH, Siswandono. Synthesis and in vitro cytotoxicity of 1-Benzoyl-3-Methylthiourea derivatives. Procedia Chem. 2015;17(1):157-61. DOI: 10.1016/j.proche.2015.12.105.

18. Morphet B, Rees SWP, Haverkate NA, Aziz H, Leung E, Pilkington LI, et al. Synthesis and Anti-Proliferative Activity of 5-Benzoyl and 5-Benzylhydroxy Derivatives of 3-Amino-2-Arylcarboxamido-Thieno[2-3-b]Pyridines. Int J Mol Sci. 2023;24(14):11407. DOI: 10.3390/ijms241411407; PMID: 37511173; PMCID: PMC10380547.

19. Khedraoui M, Abchir O, Nour H, Yamari I, Errougui A, Samadi A, et al. An In Silico Study Based on QSAR and Molecular Docking and Molecular Dynamics Simulation for the Discovery of Novel Potent Inhibitor against AChE. Pharmaceuticals. 2024;17(7):830. DOI: 10.3390/ph17070830; PMID: 39065681; PMCID: PMC11280381.

20. Pires DE, Blundell TL, Ascher DB. pkCSM: Predicting Small-Molecule Pharmacokinetic and Toxicity Properties Using Graph-Based Signatures. J Med Chem. 2015;58(9):4066-72. DOI: 10.1021/acs.jmedchem.5b00104; PMID: 25860834; PMCID: PMC4434528.

21. Pratama MRF, Poerwono H, Siswodihardjo S. Molecular docking of novel 5-O-benzoylpinostrobin derivatives as wild type and L858R/T790M/V948R mutant EGFR inhibitor. J Basic Clin Physiol Pharmacol. 2019;30(6):20190301. DOI: 10.1515/jbcpp-2019-0301; PMID: 31855568.

22. Pratama MRF, Poerwono H, Siswandono S. Design and Molecular Docking of Novel 5-O-Benzoylpinostrobin Derivatives as Anti-Breast Cancer. Thai J Pharm Sci. 2019;43(4):201-12. DOI: 10.56808/3027-7922.3054

23. Pratama MRF, Poerwono H, Siswodiharjo S. ADMET properties of novel 5-O-benzoylpinostrobin derivatives. J Basic Clin Physiol Pharmacol. 2019;30(6):20190251. DOI: 10.1515/jbcpp-2019-0251; PMID: 31851612.

24. Castro-Alvarez A, Costa AM, Vilarrasa J. The Performance of Several Docking Programs at Reproducing Protein-Macrolide-Like Crystal Structures. Molecules. 2017;22(1):136. DOI: 10.3390/molecules22010136; PMID: 28106755; PMCID: PMC6155922.

25. Claveria-Gimeno R, Vega S, Abian O, Velazquez-Campoy A. A look at ligand binding thermodynamics in drug discovery. Expert Opin Drug Discov. 2017;12(4):363-77. DOI: 10.1080/17460441.2017.1297418; PMID: 28276703.

26. Attaallah R, Amine A. The Kinetic and Analytical Aspects of Enzyme Competitive Inhibition: Sensing of Tyrosinase Inhibitors. Biosensors. 2021;11(9):322. DOI: 10.3390/bios11090322; PMID: 34562912; PMCID: PMC8471001.

27. Hall J. A simple model for determining affinity from irreversible thermal shifts. Protein Sci. 2019;28(10):1880-7. DOI: 10.1002/pro.3701; PMID: 31361943; PMCID: PMC6739816.

28. Wan S, Bhati AP, Zasada SJ, Coveney PV. Rapid, accurate, precise and reproducible ligand-protein binding free energy prediction. Interface Focus. 2020;10(6):20200007. DOI: 10.1098/rsfs.2020.0007; PMID: 33178418; PMCID: PMC7653346.

29. Gimeno A, Delgado S, Valverde P, Bertuzzi S, Berbís MA, Echavarren J, et al. Minimizing the Entropy Penalty for Ligand Binding: Lessons from the Molecular Recognition of the Histo Blood-Group Antigens by Human Galectin-3. Angew Chem Int Ed Engl. 2019;58(22):7268-72. DOI: 10.1002/anie.201900723; PMID: 30942512; PMCID: PMC6619289.

30. Lam TP, Tran NN, Pham LD, Lai NV, Dang BN, Truong NN, et al. Flavonoids as dual-target inhibitors against α-glucosidase and α-amylase: a systematic review of in vitro studies. Nat Prod Bioprospect. 2024;14(1):4. DOI: 10.1007/s13659-023-00424-w; PMID: 38185713; PMCID: PMC10772047.

31. Badukle H, Jawarkar RD, Shah U, Chaudhary S, Alzahrani AYA, Samad A, et al. From in-silico QSAR modeling to in-vitro MTT assay: experimental validation of novel uPAR leads for triple-negative breast cancer (TNBC) and skin cancer. Sci Rep. 2026;16(1):5786. DOI: 10.1038/s41598-026-36406-4; PMID: 41559139; PMCID: PMC12894839.

32. Decherchi S, Cavalli A. Thermodynamics and Kinetics of Drug-Target Binding by Molecular Simulation. Chem Rev. 2020;120(23):12788-833. DOI: 10.1021/acs.chemrev.0c00534; PMID: 33006893; PMCID: PMC8011912.

33. Savale RU, Bhowmick S, Osman SM, Alasmary FA, Almutairi TM, Abdullah DS, et al. Pharmacoinformatics approach based identification of potential Nsp15 endoribonuclease modulators for SARS-CoV-2 inhibition. Arch Biochem Biophys. 2021;700:108771. DOI: 10.1016/j.abb.2021.108771; PMID: 33485847; PMCID: PMC7825923.

34. Artamonov DV, Popova PI, Korf EA, Voitenko NG, Chernysheva AA, Avdonin PV, et al. Interpretable Machine Learning with SHAP Identifies Key Biomarkers in a Multi-Factorial Spectrum of Age-Related Neurological and Metabolic Conditions. Int J Mol Sci. 2026;27(4):1805. DOI: 10.3390/ijms27041805; PMID: 41751941; PMCID: PMC12941188.

35. Gupta KM, Chin X, Kanaujia P. Molecular Interactions between APIs and Enteric Polymeric Excipients in Solid Dispersion: Insights from Molecular Simulations and Experiments. Pharmaceutics. 2023;15(4):1164. DOI: 10.3390/pharmaceutics15041164; PMID: 37111649; PMCID: PMC10143979.

36. Tahiroğlu V, Gören K, Kotan G, Yüksek H. Correction: In silico drug evaluation by molecular docking, ADME studies and synthesis, characterization, biological activities, DFT, SAR analysis of the novel Mannich bases. BMC Chem. 2025;19(1):265. DOI: 10.1186/s13065-025-01644-6; PMID: 41024197; PMCID: PMC12477802.